

Variation in glass transition temperature of polymer nanocomposite films driven by morphological transitions

Sivasurender Chandran, J. K. Basu, and M. K. Mukhopadhyay

Citation: *J. Chem. Phys.* **138**, 014902 (2013); doi: 10.1063/1.4773442

View online: <http://dx.doi.org/10.1063/1.4773442>

View Table of Contents: <http://jcp.aip.org/resource/1/JCPSA6/v138/i1>

Published by the [American Institute of Physics](#).

Additional information on *J. Chem. Phys.*

Journal Homepage: <http://jcp.aip.org/>

Journal Information: http://jcp.aip.org/about/about_the_journal

Top downloads: http://jcp.aip.org/features/most_downloaded

Information for Authors: <http://jcp.aip.org/authors>

ADVERTISEMENT



Goodfellow
metals • ceramics • polymers • composites
70,000 products
450 different materials
small quantities fast

www.goodfellowusa.com

Variation in glass transition temperature of polymer nanocomposite films driven by morphological transitions

Sivasurender Chandran,¹ J. K. Basu,^{1,a)} and M. K. Mukhopadhyay²

¹Department of Physics, Indian Institute of Science, Bangalore, 560 012, India

²Applied Materials Science Division, Saha Institute of Nuclear Physics, Kolkata, 700 064, India

(Received 2 September 2012; accepted 12 December 2012; published online 7 January 2013)

We report the variation of glass transition temperature in supported thin films of polymer nanocomposites, consisting of polymer grafted nanoparticles embedded in a homopolymer matrix. We observe a systematic variation of the estimated glass transition temperature T_g , with the volume fraction of added polymer grafted nanoparticles. We have correlated the observed T_g variation with the underlying morphological transitions of the nanoparticle dispersion in the films. Our data also suggest the possibility of formation of a low-mobility glass or gel-like layer of nanoparticles at the interface, which could play a significant role in determining T_g of the films provided. © 2013 American Institute of Physics. [<http://dx.doi.org/10.1063/1.4773442>]

I. INTRODUCTION

Polymer thin films have been extensively studied in the last two decades to explore the possibility of finding a length scale underlying glass formation in polymers.^{1–8} Several review articles summarize our current understanding of the subject.^{9,10} Despite, a large body of work suggesting the existence of a finite size effect on glass transition temperature, T_g , of polymers, several examples contradicting the results exist in literature² so that the outcome of an enormous amount of research in the last two decades is inconclusive on this aspect. It is clear that part of this discrepancy stems from the significant contribution of surface/interface effects along with possible finite size effects. An alternative method to explore possible finite size effects as well as the role of the interface on polymer thermo-mechanical properties is to impregnate it with nanoparticles.^{7,11–13} Equivalence of the perturbation of the bulk glass transition of polymers when confined in the form of thin films or impregnation with nanoparticles has been demonstrated.^{11–13} A large body of work in the area of polymer nanocomposites (PNC) has emerged in the last decade,^{11–17} driven not only to explore the finite size and interface effects on polymer physical properties, but also to create new materials with novel physical properties. A crucial aspect in determining the ultimate success of this strategy, and hence to maximize the benefits of the anticipated electrical, optical, and magnetic properties,¹⁸ is the ability to tune the dispersion of the particles in the embedded polymer matrices, and to prevent the thermal degradation of the polymer matrix. Although research^{11–13} seems to indicate T_g variation with increase in volume fraction of added particles, some recent work seems to indicate no T_g variation in PNCs.¹⁹ A successful dispersion strategy has been to use polymer grafted nanoparticles (PGNP) in the identical polymer matrix to create an athermal blend.^{5,11–13,20} The morphological phase diagrams of such blends are beginning to be elucidated.^{20–28} However, very few studies have been made on the physical

properties especially on their glass transition.^{14,15} Needless to say that, for various practical applications such composites will eventually have to be prepared in the form of a film or a coating. Thus, studying the properties of thin films of these materials is of vital importance. However, it turns out that the interface plays a crucial role in such thin films,^{14,15} to the extent that the nature of dispersion in the bulk could be significantly modified. The film and substrate processing conditions, which are crucial for thin polymer films, turn out to be much more critical in PNC thin films.²⁹ These in turn could lead to large changes in thermo-mechanical properties of thin films of PNCs as well. Therefore, to explore the interplay of strong confinement of polymer segments by embedded nanoparticles at high volume fractions and the surface effects, especially the role of particle dispersion, we have studied the glass transition of PGNP embedded PNC thin films.

Here, we report a comprehensive measurement, following up on our earlier work¹⁵ of T_g variation in polystyrene films of thickness ~ 70 nm embedded with thiol terminated polystyrene (PST) capped gold nanoparticles (Au NP) of fixed size and various properties as shown in Table I. The volume fraction of the embedded gold in the polymer matrix, ϕ_p has been varied from 0.1–10, as indicated in Table II. We have estimated the T_g variation from the temperature dependence of film thickness using spectroscopic ellipsometry and correlated this variation with the detailed three-dimensional morphology of the film using atomic force microscopy (AFM), field emission scanning electron microscope (FESEM), and X-ray reflectivity (XRR). We observe step-wise decrease in T_g of the polymer films as a function of added PGNP. We provide a model for this T_g variation in terms of the underlying morphological phase transition in the dispersion of PGNPs and also allude to the existence of possible viscosity gradient along the film thickness similar to the recent observations.^{3,17} The overall impact of particle loading, morphological transitions, processing conditions, and possible viscosity gradients on T_g variation of PNC thin films are discussed.

^{a)}E-mail: basu@physics.iisc.ernet.in.

TABLE I. Properties of PGNP.

Sample	R_c nm	Σ nm	σ Chains/nm ²	R_c nm	R_c/R_g
PST-Au	2.1 ± 0.2	1.5	1.98 ± 0.2	3.6	0.45

II. EXPERIMENTAL DETAILS

Polymer grafted nanoparticles consisting of a core of gold nanoparticles (Au NP) and corona of thiol terminated polystyrene (PST of molecular weight 3 Kg/mol, degree of polymerization $N \sim 27$), grafted to the Au NP core, were synthesized by a method described earlier.^{15,20,22,30,31} Transmission electron microscopy (TEM, Technai, T20) and thermogravimetric analysis (TGA, METTLER) were used to estimate the grafting density σ of the PST chains on PGNP core. The average thickness of the PST shell, Σ on the Au NPs has been estimated to be ~ 1.5 nm from inter-particle spacings obtained from TEM images. The total radius of the PGNP $R_c (= \Sigma + R_e, R_e$ is the radius of the PGNP core) is therefore estimated to be ~ 3.6 nm. PGNP solutions were mixed with the polystyrene (PS) (molecular weight 97.4 Kg/mol, degree of polymerization $P \sim 936$; radius of gyration, $R_g = 8$ nm) solutions in appropriate ratios as indicated in Table II. The mixtures were stirred for ~ 24 h to ensure the formation of a homogeneous dispersion. Thin films of these PGNP-polymer suspension were then prepared (using the solutions mentioned above) on polished silicon wafers (Vin Karola Inc, USA) cleaned using standard methods described earlier.¹⁵ The films were annealed at $\sim 150^\circ\text{C}$ (well above the T_g of bulk PS ($T_g^{bulk} = 105^\circ\text{C}$ as well as for a PS film of thickness ~ 70 nm, $T_g^{film} = 106^\circ\text{C}$) for 12 h in a vacuum better than $\sim 8 \times 10^{-3}$ mbar, to ensure the removal of trapped solvent and the equilibration of the matrix chains along with an equilibrium particle dispersion. The thickness of the films were 70 ± 5 nm at 27°C , as measured by spectroscopic ellipsometry (SE850, Sentech, Germany). Glass transition T_g^{bulk} of PS and polymer nanocomposite powders, thermally annealed in identical manner to the corresponding thin films, were measured using modulated differential scanning calorimetry (MDSC) measurements (TA Instruments) as described earlier.¹¹ Temperature dependent spectroscopic ellipsometric measurements were performed on the samples specified in Table II using a home-made high temperature sample chamber evacuated to

TABLE II. Specification of PGNP-PS hybrid films.

Sample	Volume fraction (Percentage) ϕ_p	Weight fraction (Percentage)
S1	0.1	1.8
S2	0.3	5.2
S3	0.75	12.0
S4	1.2	17.9
S5	3.0	34.8
S6	5.0	46.6
S7	10.0	62.3

$\sim 3 \times 10^{-2}$ mbar. The chamber, especially the quartz windows used in the beam path, were tested for appearance of the possible spurious polarization changes from residual stress due to temperature variation.

X-ray reflectivity measurements on the samples, described in Table II, were performed at BL 18B in Photon Factory synchrotron, Tsukuba, Japan, at an incident x-ray energy of 10 KeV as well as with a D8 Discover lab based reflectometer (Bruker, Germany) at 8 KeV. The electron density profiles (EDP) $\rho(z)$ of the various PNC films were extracted from the measured reflectivity, R , as a function of the perpendicular wave vector transfer, $q_z (= 4\pi \sin\theta/\lambda$, where θ and λ are the angle of incidence and wavelength of the incident x-rays on the samples). Atomic force microscopy (NT-MDT, NTEGRA) measurements were performed, in contact mode using NT-MDT cantilevers to find the surface morphology. The lateral dispersions of particles were seen using FESEM (Ultra Zeiss, Germany), operated at 8 keV with a working distance of 3 mm.

III. RESULTS AND DISCUSSIONS

A. Glass transition

For estimating the T_g of PNC films, they were heated to 150°C (at a vacuum better than $\sim 3 \times 10^{-2}$ mbar) and held at this temperature for 2 h to maintain equilibrium conditions in the sample. Ellipsometric angles Ψ and Δ were measured, *in situ*, continuously from 150°C to room temperature, over a wavelength range of 300–600 nm, at a cooling rate of $\sim 0.8^\circ\text{C}/\text{min}$. The film thickness was determined by fitting the ellipsometric angles, over the entire range of wavelengths stated above, with a Maxwell-Garnett effective medium model of dispersion of gold in a Cauchy layer of the polymer.¹⁵ Typical plots of thickness vs temperature, along with the estimation of T_g , is shown in Fig. 1. The clear variation of T_g with ϕ_p is evident from the four ellipsometry data.

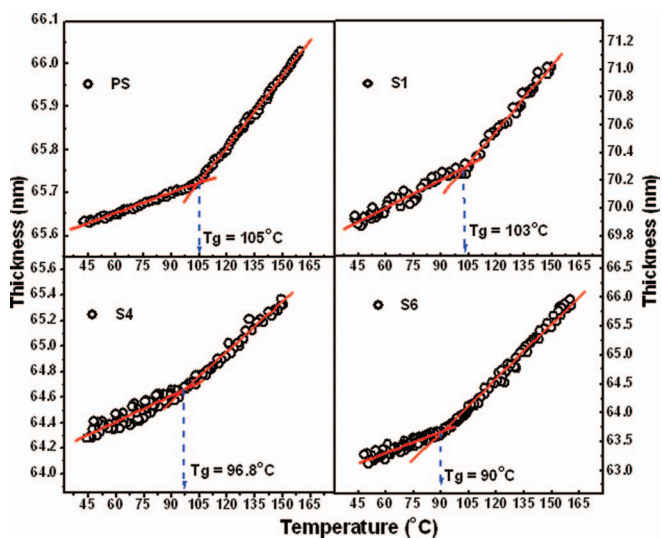


FIG. 1. Thickness vs temperature for samples S1, S4, S6, and PS thin film of thickness 65 nm as indicated in the respective panels. The continuous lines (red) are the linear fits in the respective regions, with the T_g indicated by the vertical dashed lines in each panel.

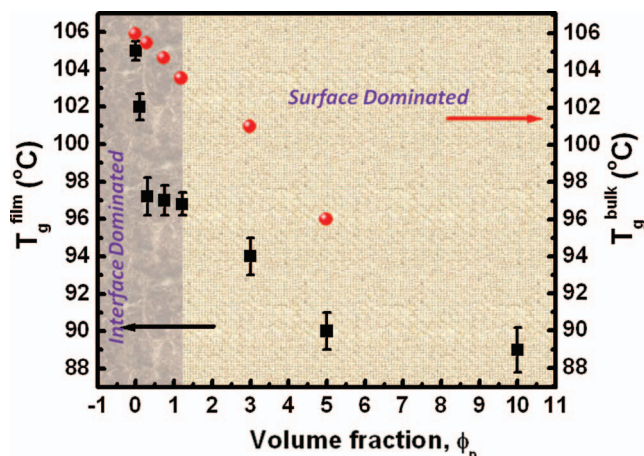


FIG. 2. Glass transition temperature T_g , in both bulk (circle) and in the thin films (square), is shown as a function of the volume fraction of added PGNPs, ϕ_p . The interpretation for the T_g variation for different ϕ_p values is discussed in details in the text.

The variation of T_g of all the PNC, as well as PS films, is summarised in Fig. 2. Also shown in the same plot is the nature of variation of T_g of the PNC powders, measured using MDSC, with ϕ_p . Reduction in T_g with increasing ϕ_p for both the bulk and the thin film samples is clearly visible. The general overall trend of reduction in T_g of the PNC (both bulk and thin films) is consistent with the bulk measurements and some of the earlier observations in PNC powders^{11–13} and thin films.^{14,15} Especially, for PNCs where $N \ll P$, it is expected^{11–15,25,26} that the matrix chains would be repelled from the particle interface leading to enhanced segmental mobility at the interface and hence overall reduction in T_g . However, what is interesting in our case for the PNC thin films is the observation of an intermediate range of ϕ_p values, where T_g of the films, is independent of ϕ_p , whereas for the bulk PNC powders the T_g variation with ϕ_p is monotonic. It might also be noted that for a very similar system, Green *et al.*,¹⁴ have obtained considerably larger T_g deviation at comparable volume/weight fractions (sample C in Ref. 14 and S2 in our case). One major difference is the different annealing conditions used and we have shown earlier¹⁵ how morphology, dispersion, and T_g depend on annealing conditions. The role of interfacial interactions as described earlier can be very important and especially, for PGNP-polymer blends, a first order transition leading to the interfacial segregation of particles can take place.²³ To rationalize the observed behavior in T_g , detailed structure and morphology of the PGNP-polymer blend films have been studied with AFM, FESEM, as well as XRR.

B. Structure

In Fig. 3, the AFM images of some of the films (after annealing) used in this work are shown. At lower ϕ_p , the PGNPs seem to be very well dispersed (S1), with the fraction of particles at the surface increasing with increase in ϕ_p . At higher fractions viz., $\phi_p = 10$ (considerably higher than the volume fractions used in most earlier studies^{14,15}), PGNPs started forming percolated networks at the surface. In Fig. 4, AFM images of the various PNC films before (vacuum dried at

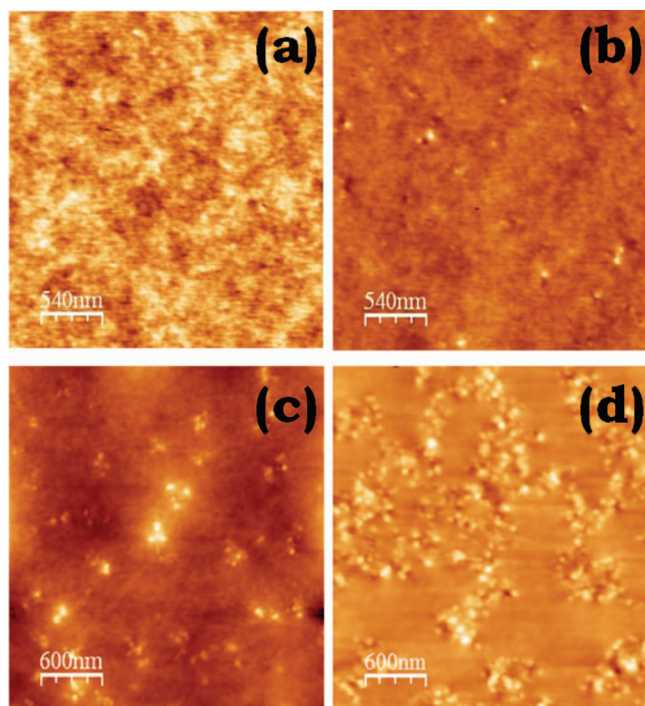


FIG. 3. AFM images of the samples S1 (a), S3 (b), S5 (c), and S7 (d) after annealing (see text for details).

70 °C) and after annealing are compared to illustrate the role of annealing. It is clear from this comparison that there is a considerable redistribution of particles during annealing from the highly non-equilibrium kinetic structure and morphology acquired during the spin coating process. Field emission scanning electron microscope images (Fig. 5) further confirm the surface morphological features observed in AFM and also indicate the morphology slightly below the surface. Especially, for sample S5 it appears that the network-like structure is only present at the surface and not in the bulk. What about the morphology at the film-substrate interface?

To understand this, we have used XRR measurements on these films as shown in Fig. 6. The inset highlights the key

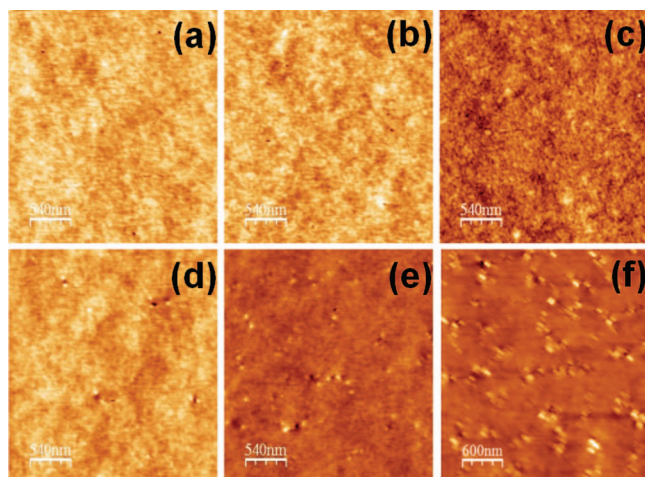


FIG. 4. AFM images of un-annealed [(a)–(c)] and annealed [(d)–(f)] samples S2, S4, and S6, respectively. Variation of surface morphology, and redistribution of particles with annealing, is evident.

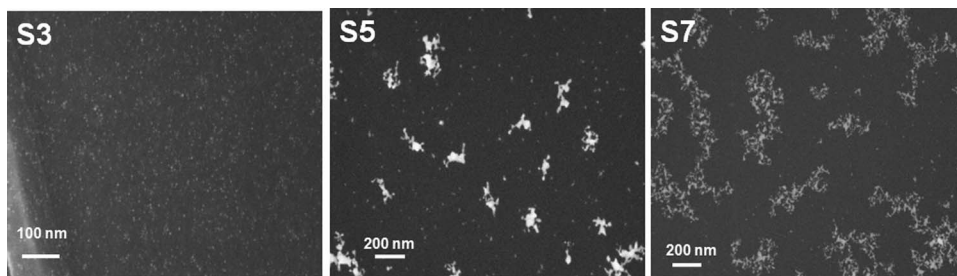


FIG. 5. FESEM images showing the lateral dispersion of three different samples as identified in the figure. Percolation of the particles at the surface and the dispersion in the bulk (regions with the lesser contrast) could be noticed.

signature of a structural transition taking place in these films at and above a certain volume fraction $\phi_p = 0.75$, similar to earlier observations.²³ The transition is indicative of interface segregation. To quantify the segregation, the XRR profiles (R Vs q_z) were modeled with a three slab model. The corresponding EDP as obtained (from the fits shown in Fig. 6) is shown in Fig. 7(a). The depth profile of PGNP, more specifically depth profile of the gold, $\phi_{Au}(z)$, as extracted from the EDP, is shown in Fig. 7(b). It is clear that there is no significant surface or interface segregation up to $\phi_p = 0.3$ but from $\phi_p = 0.75$ there is a considerable PGNP segregation at the film substrate interface. It seems that the interface segregation starts at some ϕ_p , $0.3 < \phi_p < 0.75$. Curiously, this is also the volume fraction, which falls in the plateau region of T_g variation of the films. Is there a connection between these two? It seems (Fig. 7(b)) that while the surface and bulk fractions of PGNP increase rather continuously, the interface density varies in a discontinuous manner. The nature of surface PGNP density variation obtained from XRR analysis is consistent

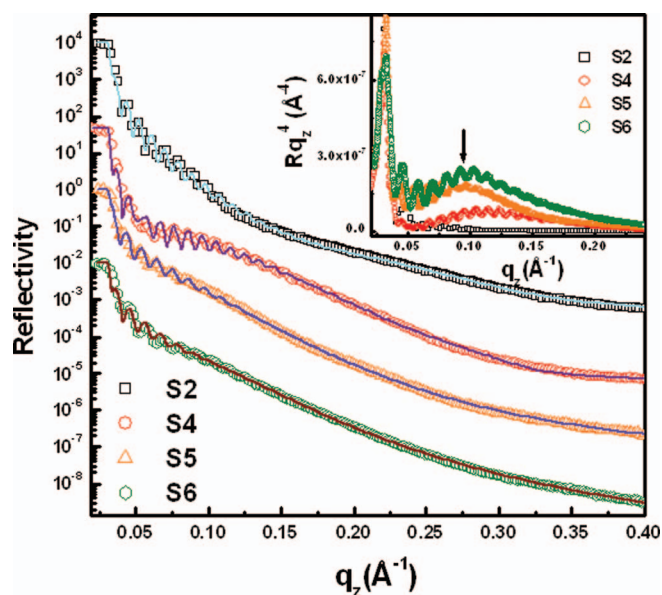


FIG. 6. Reflectivity profiles, R vs q_z for some of the samples along with the fits (solid lines) to the data (open symbols). Inset: Normalized XRR profile (Rq_z^4 vs q_z) indicative of the presence of electron density modulation over and above the homogeneous dispersion of PGNPs. The peak position as indicated by an arrow can be used as a possible estimate of the length scale over which the electron density modulates. The XRR profiles have been shifted vertically by an arbitrary factor for clarity.

with the AFM and FESEM images. To further quantify the nature of dispersion of PGNPs, we have calculated the mean surface-surface separation, h , at various locations within the PNC films. From Fig. 8, it can be seen clearly that h (h_{int} , h_{bulk} , and h_{surf}) decreases with increasing ϕ_p as expected. However, for $\phi_p = 3$, although both h_{surf} and h_{bulk} were greater than Σ ; we start seeing the formation of percolated clusters at the surface, where as PGNPs in the bulk stays dispersed (Fig. 5). Since the complete 3-dimensional structure and morphology of the PGNP in these PGNP-polymer blend films could be obtained, can we use this to rationalize the observed T_g variation as shown in Fig. 2?

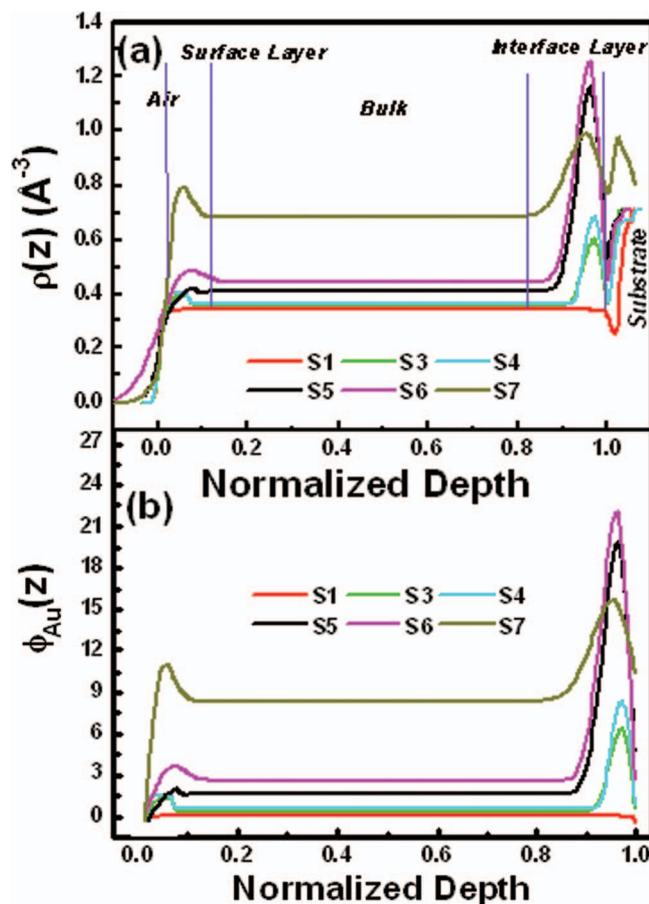


FIG. 7. Electron density profile, EDP, $\rho(z)$ (a) and volume fraction of gold $\phi_{Au}(z)$ (b) as a function of normalized depth. The nature of dispersion of PGNPs, and its variation (interface and surface segregation) with increasing ϕ_p , is clearly seen.

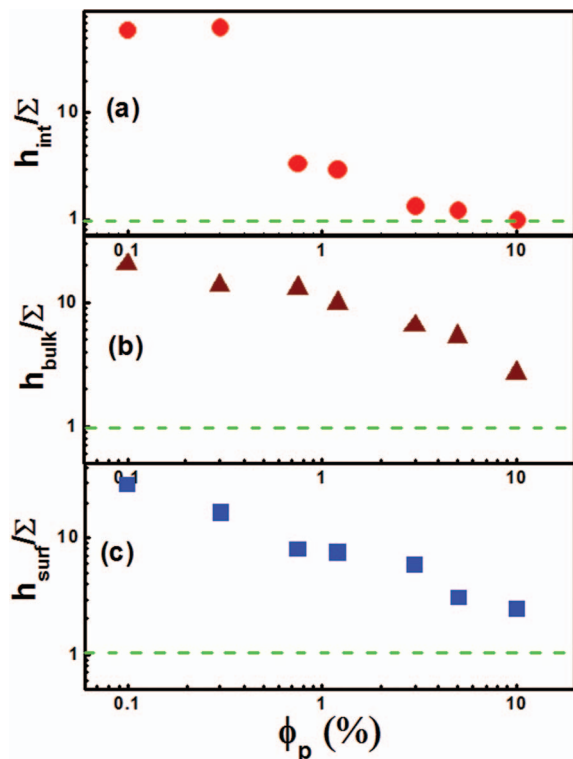


FIG. 8. Surface to surface separation (h) of the particle normalized to corona thickness (Σ) is plotted for interface (a), bulk (b), and the surface (c) layer as a function of ϕ_p . Dashed lines in panels show the point at which the inter-particle spacing “ h ,” is equal to the corona thickness Σ corresponding to maximum h close packing of PGNP, without the significant compression of the grafted chains.

C. Discussions

We propose the following model to explain the observed T_g variation and show how it can be tailored in such hybrid films by controlling its internal and interfacial morphology. In Fig. 2, the initial decrease in T_g with ϕ_p can be understood in terms of finite size effect on polymer T_g , due to the confinement of segments between PGNPs coupled with an expected enhanced segmental mobility at the de-wetting PS-PGNP interface.^{12,13,32,33} However, the magnitude of reduction in T_g is considerably lesser than the variation observed by Green *et al.*,¹⁴ which could possibly be because of the different annealing conditions as already discussed. Between $\phi_p = 0.3$ – 1.2 , T_g hardly changes although the fraction of PGNP in the bulk increases and the T_g in the bulk decreases continuously. This, we believe, is due to the competing effects on T_g variation between the interface layer, which possibly enhances the T_g and the bulk layer that decreases T_g . If the particles dispersed in the bulk has to dominate then we should have seen a decrease in T_g , but there is no variation. With these, we could conclude that T_g in this region of the volume fraction is dominated by the PGNPs segregated to the interface (interface dominated, Fig. 2). At $\phi_p = 3$, the T_g starts decreasing again due to the fact that the percentage increase in bulk fraction of PGNPs is larger than at the interface. With further increase in ϕ_p , the interface layer saturates, but more particles started diffusing in to the surface (Figs. 3–5) forming percolated domains. The formation of percolated domains

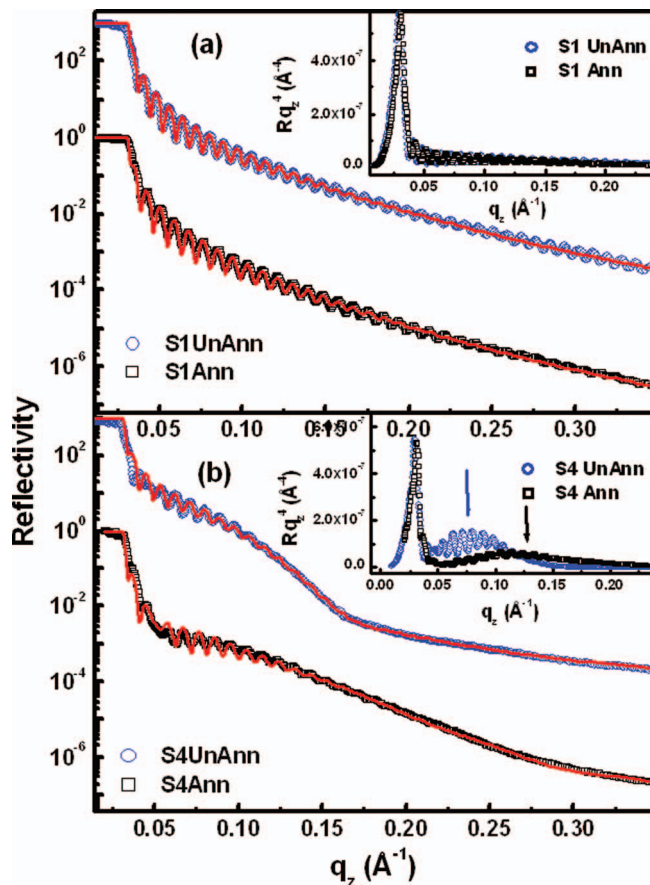


FIG. 9. Comparison between the XRR data for samples S1 (a) and S4 (b) before (open squares) and after (open circles) annealing along with the best possible fits (solid lines). Inset: Normalized reflectivities, (Rq_z^4 vs q_z), for the same data shown in the main panels (a) and (b). In both panels (a) and (b), the XRR profiles have been shifted vertically by an arbitrary factor for clarity.

hints at the reduced viscosity and T_g in the surface. So, the interface layer does not cause an additional increase of T_g , but both the PGNPs dispersed in the bulk and the surface decrease the T_g and hence T_g starts decreasing again. This is the case till S6. However, for S7, the total fraction in the film is considerably high so that a transition to a percolating network at the surface, and possibly to some extent in the bulk, takes place. This is also clear from the magnitude of mean surface-surface separation of PGNP (Figs. 8(a)–8(c)) in the three layers compared to Σ for all the samples especially, S6 and S7. To obtain a further insight regarding the effect of interface layer of PGNP on T_g , we explore the possibility to estimate the effective particle mobility in this interface layer.

In Fig. 9, we have shown a comparison of XRR data for two samples S1 and S4 before and after annealing. For sample S1, the difference in the reflectivity between the annealed and un-annealed film appears to be small and becomes evident only by taking a close look at the Fresnel normalised profiles in inset of Fig. 9(a). However, for sample S4, the difference in XRR profiles, and especially the normalised profiles (inset of 9(b)), clearly reveals a considerable re-organisation of the PGNP distribution within the films during annealing. Detailed analysis of the XRR profiles leads to the respective volume fraction distribution for gold within the films as shown

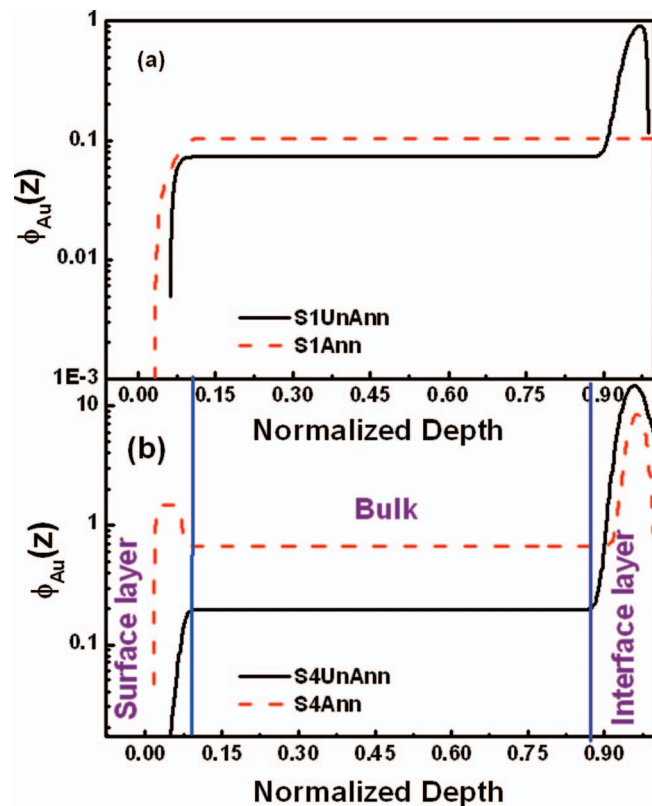


FIG. 10. Volume fraction of gold $\phi_{Au}(z)$ as a function of normalized depth for samples S1 (a) and S4 (b) with (dashed line) and without annealing (continuous line). The preferential segregation of the particles to the interface even in the un-annealed films can be noticed.

in Fig. 10. It is clear that the interface layer is formed in these thin films during spin coating and even without annealing, although the extent of such segregation is considerably higher in S4 than in S1. Interestingly, while for S1 annealing at temperatures $T \gg T_g$ does seem to re-disperse all the interface PGNPs into the bulk, for S4 dispersion is incomplete, although the thickness and the density of this interface PGNP layer does decrease. The AFM images in Fig. 4 also confirm this conclusion regarding PGNP dispersion. We believe that the structural transition leading to the formation of a stable interface layer of PGNPs could also lead to the formation of high viscous glassy layer in which the mobility of the PGNPs is reduced to such an extent that it cannot be re-dispersed into the bulk despite long-time annealing at temperature $T \gg T_g$. This in turn would lead to the reduced mobility of polymers not only in the interface layer, but also in the adjoining layers. The effective T_g of this layer could thus be expected to be higher than bulk T_g of PS. This is also along the lines of some recent suggestions^{3,17} indicating a higher viscous dead interface polymer layer, although the mechanism is different in our case. The T_g would then be determined by the competition between the enhanced segmental mobility of the PGNP interface in the bulk and the reduced mobility near the substrate interface pinned PGNP layer. It turns out that ϕ_{Au} increases across the thickness of the film after annealing, while it decreases at the interface layer. However, the relative increase of ϕ_{Au} is more in the surface as compared to the bulk, which is indicative of a higher mobility of the PGNP and hence a lower

effective viscosity at the surface. We feel that the surface layer has higher mobility and lower viscosity than the bulk, along the lines of several recent suggestions.^{34,35} Further, the fact that PGNP network formation seems to be considerably more prominent at the surface (Figs. 3–5) compared to bulk also points to the possibility of enhanced surface mobility. We believe the repulsive PGNP-polymer interaction, coupled with the reduced effective viscosity of the surface polymer layer, leads to the enhanced probability of PGNP network formation at the surface. However, we do not have a quantification of this reduction at this point of time, but our claim seems to be backed up by some recent studies.¹⁷

IV. CONCLUSIONS

In conclusion, we have demonstrated direct correlation between morphological transition in the interior of a PNC film with the variation of its T_g , over a large range of PGNP volume fraction. Complex interplay between finite size effects, mediated by inter-particle separations and the dispersion of PGNPs, leads to a step-wise discontinuous variation in T_g . We also believe that there are indications from our data that the structural transition, which drives PGNP segregation to the film-substrate interface, leads to the formation of a layer of low mobility of PGNP, which could have glass or gel-like behavior. We further demonstrate the synergy in NP-polymer blends and their thin films which cannot only be used to control the properties of the blend, along with the interaction with the substrate, but the embedded NP, can also be used as an effective nanoscale probe of the local thermo-mechanical and rheological properties of highly confined polymer films. These findings will also have broader implications in the better understanding of the confinement effects on glass transition temperature, self assembly, and dispersion of nanoparticles and their applications. More work is in progress to understand the role of dispersion and effect of confinement in similar systems.

ACKNOWLEDGMENTS

The authors would like to acknowledge DST, India and SINP, India for providing the funding for XRR measurements in Photon Factory, Tsukuba, Japan. The authors would also like to acknowledge the Institute Nanoscience Initiative (INI), IISc for providing access to TEM facility and to the Center for Excellence in Nanoscience and Engineering (CeNSE), IISc for providing access to FESEM facility.

- ¹J. L. Keddie, R. A. Jones, and R. A. Cory, *Europhys. Lett.* **27**, 59 (1994).
- ²M. Tress, M. Erber, E. U. Mapesa, H. Huth, J. Muller, A. Serghei, C. Schick, K.-J. Eichhorn, B. Voit, and F. Kremer, *Macromolecules* **43**, 9937 (2010).
- ³S. Napolitano and M. Wubbenhorst, *Nat. Commun.* **260**, 2 (2011).
- ⁴Z. Fakhraei and J. A. Forrest, *Science* **319**, 600 (2008).
- ⁵V. M. Boucher, D. Cangialosi, A. Alegria, J. Colmenero, I. Pastoriza-Santos, and L. M. Liz-Marzand, *Soft Matter* **7**, 3607 (2011).
- ⁶V. Pryamitsyn and V. Ganesan, *Macromolecules* **43**, 5851 (2010).
- ⁷J. M. Kropka, V. Pryamitsyn, and V. Ganesan, *Phys. Rev. Lett.* **101**, 075702 (2008).
- ⁸K. J. Lee, D. K. Lee, Y. W. Kim, W. Choe, and J. H. Kim, *J. Polym. Sci., Part B: Polym. Phys.* **45**, 2232 (2007).

- ⁹M. Alcoutlabi and G. B. McKenna, *J. Phys.: Condens. Matter* **17**, 461 (2005).
- ¹⁰J. A. Forrest and K. Dalnoki-Veress, *Adv. Colloid Interface Sci.* **94**, 167 (2001).
- ¹¹S. Srivastava and J. K. Basu, *Phys. Rev. Lett.* **98**, 165701 (2007).
- ¹²A. Bansal, H. Yang, C. Li, K. Cho, B. C. Benicewicz, S. K. Kumar, and L. S. Schadler, *Nature Mater.* **4**, 693 (2005).
- ¹³A. Bansal, H. Yang, C. Li, B. C. Benicewicz, S. K. Kumar, and L. S. Schadler, *J. Polym. Sci., Part B: Polym. Phys.* **44**, 2944 (2006).
- ¹⁴A. Arceo, L. Meli, and P. F. Green, *Nano Lett.* **8**, 2271 (2008).
- ¹⁵S. Chandran and J. K. Basu, *Eur. Phys. J. E* **34**, 99 (2011).
- ¹⁶T. Koga, C. Li, M. K. Endoh, J. Koo, M. Rafailovich, S. Narayanan, D. R. Lee, L. B. Lurio, and S. K. Sinha, *Phys. Rev. Lett.* **104**, 066101 (2010).
- ¹⁷T. Koga, N. Jiang, P. Gin, M. K. Endoh, S. Narayanan, L. B. Lurio, and S. K. Sinha, *Phys. Rev. Lett.* **107**, 225901 (2011).
- ¹⁸D. Y. Godovsky, *Adv. Polym. Sci.* **153**, 163 (2000).
- ¹⁹J. S. Meth, S. G. Zane, C. Chi, J. D. Londono, B. A. Wood, P. Cotts, M. Keating, W. Guise, and S. Weigand, *Macromolecules* **44**, 8301 (2011).
- ²⁰S. Chandran, C. K. Sarika, A. K. Kandar, J. K. Basu, S. Narayanan, and A. Sandy, *J. Chem. Phys.* **135**, 134901 (2011).
- ²¹E. S. McGarrity, P. M. Duxbury, M. E. Mackay, and A. L. Frischknecht, *Macromolecules* **41**, 5952 (2008).
- ²²M. K. Corbierre, N. S. Cameron, M. Sutton, S. G. Mochrie, L. B. Lurio, A. Ruhm, and R. B. Lennox, *J. Am. Chem. Soc.* **123**, 10411 (2001).
- ²³E. S. McGarrity, A. L. Frischknecht, L. J. D. Frink, and M. E. Mackay, *Phys. Rev. Lett.* **99**, 238302 (2007).
- ²⁴A. Chremos, A. Z. Panagiotopoulos, H. Yu, and D. L. Koch, *J. Chem. Phys.* **135**, 114901 (2011).
- ²⁵V. Ganesan, C. J. Ellison, and V. Pryamitsyn, *Soft Matter* **6**, 4010 (2010).
- ²⁶L. Meli, A. Arceo, and P. F. Green, *Soft Matter* **5**, 533 (2009).
- ²⁷P. Akcora, H. Liu, S. K. Kumar, J. Moll, Y. Li, B. C. Benicewicz, L. S. Schadler, D. Acehan, A. Z. Panagiotopoulos, V. Pryamitsyn, V. Ganesan, J. Ilavsky, P. Thiyagarajan, R. H. Colby, and J. F. Douglas, *Nature Mater.* **8**, 354 (2009).
- ²⁸D. Dukes, Y. Li, S. Lewis, B. Benicewicz, L. Schadler, and S. K. Kumar, *Macromolecules* **43**, 1564 (2010).
- ²⁹A. Sergei, *Macromol. Chem. Phys.* **209**, 1415 (2008).
- ³⁰A. K. Kandar, S. Srivastava, J. K. Basu, M. K. Mukhopadhyay, S. Seifert, and S. Narayanan, *J. Chem. Phys.* **130**, 121102 (2009).
- ³¹S. Srivastava, S. Chandran, A. K. Kandar, C. K. Sarika, J. K. Basu, S. Narayanan, and A. Sandy, *J. Chem. Phys.* **133**, 151105 (2010).
- ³²F. W. Starr, T. B. Schroder, and S. C. Glotzer, *Phys. Rev. E* **64**, 021802 (2001).
- ³³J. M. Kropka, V. G. Sakai, and P. F. Green, *Nano Lett.* **8**, 1061 (2008).
- ³⁴C. R. Daley, Z. Fakhraai, M. D. Ediger, and J. A. Forrest, *Soft Matter* **8**, 2206 (2012).
- ³⁵F. Dinelli, A. Ricci, T. Sgrilli, P. Baschieri, P. Pingue, M. Puttaswamy, and P. Kingshott, *Macromolecules* **44**, 987 (2011).